Biomass and Bioenergy 199 (2025) 107911

Contents lists available at ScienceDirect

Biomass and Bioenergy

journal homepage: www.elsevier.com/locate/biombioe

Low temperature chemical looping combustion of pyrolysis gases in a fixed bed reactor

César Gracia-Monforte [a], Francisco Maldonado-Martín [a], María Atienza-Martínez [b,*], Javier Ábrego [a]

[a] Thermochemical Processes Group, Aragón Institute of Engineering Research (I3A), University of Zaragoza, Edificio I+D, Campus Rio Ebro, Zaragoza, 50018, Spain
[b] Grupo de Reactores Químicos y Procesos para la Valorización de Recursos Renovables, Institute for Advanced Materials and Mathematics (InaMat^2), Departamento de Ciencias, Edificio de los Acebos, Universidad Pública de Navarra, Campus de Arrosadía, E-31006, Pamplona, Spain

ARTICLE INFO

Keywords:
Chemical looping combustion (CLC)
Oxygen carrier (OC)
Carbon capture
Advanced combustion
Pyrolysis gas

ABSTRACT

This study presents an experimental investigation into the feasibility of oxidizing biomass pyrolysis gases at relatively low temperatures using a chemical looping combustion (CLC) approach. The application of this alternative method would enable the capture of carbon from the pyrolysis gas stream, which is currently released into the atmosphere in most pyrolysis systems, as high-purity CO_2. In a fixed bed reactor, the reduction behavior of three different Cu-based oxygen carriers (OC) - pure CuO pellets, carulite and Al_2O_3-supported CuO - was evaluated to determine whether pyrolysis gases could be completely oxidized to CO_2 and H_2O within a temperature range of 600–650 °C and at weight hourly space velocities (WHSV) of 0.06–0.10 h^{-1}. Both CuO and carulite exhibited significant amounts of unconverted pyrolysis gases even during the initial stages of the reduction experiments. In contrast, Al_2O_3-supported CuO emerged as the most effective material, facilitating the complete oxidation of pyrolysis gases over extended reaction times. For this oxygen carrier, a decline in the combustion efficiency was only observed at very high (90 %) reduction conversions. Reduction/oxidation cycles for this most promising material were successfully demonstrated, with the oxygen carrier showing no signs of activity loss after 10 cycles. However, carbon deposition was detected under several experimental conditions, which could potentially reduce the carbon capture efficiency of the process.

1. Introduction

Pyrolysis is an attractive technology for the conversion of biomass into valuable products and energy [1]. For millennia, it has been used in charcoal production and was further developed in the 19th century to support the bio-based chemical industry. After being displaced by the rise of the petrochemical industry, pyrolysis is once again gaining importance as a key alternative for the carbon-friendly production of fuels, products, and/or energy [2].

Pyrolytic thermal decomposition of biomass always yields three distinct product fractions: solid (biochar), condensable liquids (bio-oil and permanent gases. The relative proportions of these products can be adjusted within certain limits by selecting the appropriate biomass feedstock, reaction system, and operational conditions. Fast pyrolysis involves rapid heating of small biomass particles and rapid quenching of the pyrolytic vapors, aiming to maximize the liquid fraction (up to 75 % of the original feedstock mass), which consists of hundreds of organic compounds. The liquid fraction can be further upgraded into biofuels or used to obtain valuable chemicals through separation techniques [3]. In contrast, slow and intermediate pyrolysis (with the exact limit between both being unclear) use lower heating rates, typically employ larger biomass particles, and allow for longer vapor residence times in the reaction system. This favors secondary reactions among the primary thermal decomposition products, ultimately leading to similar solid (biochar) and liquid yields [1]. Regarding the third product, pyrolysis gas, it is primarily composed of H_2, CH_4, CO, and CO_2, along with trace amounts of other gases [4]. However, the exact gas composition is frequently not reported in the literature. It is generally assumed that the gases are combusted in a burner to provide, at least partially, the heat required to drive the pyrolysis reactions within the desired temperature range of 400–600 °C [5].

This article is part of a special issue entitled: Rafael Bilbao published in Biomass and Bioenergy.

* Corresponding author: Grupo de Reactores Químicos y Procesos para la Valorización de Recursos Renovables, Institute for Advanced Materials and Mathematics (InaMat^2), Departamento de Ciencias, Edificio de los Acebos, Universidad Pública de Navarra, Campus de Arrosadía, E-31006, Pamplona, Spain.
E-mail address: maria.atienza@unavarra.es (M. Atienza-Martínez).

https://doi.org/10.1016/j.biombioe.2025.107911
Received 14 February 2025; Received in revised form 16 April 2025; Accepted 16 April 2025
Available online 7 May 2025

Nomenclature

ANOVA	Analysis of variance
CLC	Chemical looping combustion
CDR	Carbon dioxide removal
CFB	Circulating fluidized bed
EDS	Energy-dispersive detector
FESEM	Field emission scanning electron microscopy
FFD	Full factorial design
H_2-TPR	Hydrogen temperature-programmed reduction
ICP-OES	Inductively coupled plasma-optical emission spectrometry
IPCC	Intergovernmental Panel on Climate Change
OC	Oxygen carrier
STP	Standard temperature and pressure
WHSV	Weight hourly space velocity
XRD	X-ray diffraction

Depending on the intended use of its products, biomass pyrolysis can be considered a carbon dioxide removal (CDR) technology. In this context, biochar production is recognized by the Intergovernmental Panel on Climate Change (IPCC) as a key method for atmospheric carbon removal that should be deployed at relevant scales [6,7]. Biochar, that can contain more than 90 % carbon [8], has gained increasing interest due to its ability to store carbon long-term when applied to soils, as well as its potential to enhance agricultural productivity under various scenarios [9]. The global biochar market has dramatically grown in recent years [10]. Instead of being directly used as a low-grade fuel, bio-oil can be processed into advanced biofuels or chemicals, or it can safely be directly sequestrated into deep geological formations. This latter solution is currently being commercially developed by Charm Industries in the United States of America (USA) [11,12]. However, none of the existing pyrolysis-based CDR technologies consider the pyrolysis gases as a potential source of sequestrable carbon. The combustion of these gases releases a significant portion of the original biomass carbon back into the atmosphere as CO_2. If pyrolysis is to be considered a true CDR technology, alternatives to releasing this carbon back to the atmosphere must be explored [13]. Based on rough estimates from studies that report gas compositions and yields, under fast pyrolysis fluidized bed conditions at 500 °C, approximately 17 % of the total biomass carbon may end up in the gases [14], while about 10 % is observed in slow pyrolysis at similar temperatures [15,16].

As an alternative to the conventional combustion of pyrolysis gases, Chemical Looping Combustion (CLC) can be applied. CLC is an innovative technology that enables complete oxidation of gaseous fuels by using a solid oxygen carrier – typically a metal oxide – that undergoes a reduction-oxidation cycle. This cycle occurs in separate reactors or stages, where the oxygen carrier reacts with the gaseous fuels and air, respectively. This approach allows for the full oxidation of fuels to CO_2 and H_2O, without mixing these combustion products with atmospheric nitrogen (N_2). As a result, a nearly pure CO_2 stream can be obtained, ready for capture after water vapor is condensed, along with process heat.

The oxygen carrier's oxidation stage is always strongly exothermic, whereas the reduction stage can be either exothermic (e.g., with Cu or Mn oxides) or endothermic (e.g., with Ni or Fe oxides) [17]. Overall, the amount of heat generated by the chemical looping system is equivalent to the heating value of the gaseous fuels, and this heat can be used in the same way as in conventional combustion. Additionally, applying a CLC process to pyrolysis gases could result in lower CO, hydrocarbons, and particulate matter emissions [18–22]. This presents an added advantage, given that the atmospheric emissions from pyrolysis facilities are becoming an increasingly important concern [4].

In summary, given the composition of pyrolysis gases (mainly H_2, CH_4, CO, and CO_2), subjecting them to CLC seems to be a feasible approach to enhance the CO_2 removal potential in pyrolysis reactors, while also generating heat that could be used to sustain the pyrolysis process [23]. Carbon capture from the gases would further contribute to the carbon storage capacity of biochar. To implement this solution, CO_2 (e.g., recirculated from the CLC system) should be used as the carrier gas, rather than N_2 or flue gases from combustion, which would hinder the capture of a pure CO_2 stream. Coupling pyrolysis with CLC of gases can be seen as a process intensification strategy for carbon capture, as an alternative to recent proposals of pyrolysis process enhancements focused on heat transfer and autothermal operation [24].

CLC technology is typically envisioned for electricity generation with integrated CO_2 capture, both in gas turbines and combined cycles [25,26]. The reactor system commonly used in CLC consists of two interconnected circulating fluidized bed (CFB) reactors. In one reactor, the oxygen carrier (OC) undergoes reduction while the fuel is oxidized, whereas in the second reactor, the OC is oxidized with air. Alternatively, packed bed CLC reactor systems can be dynamically operated in reduction/oxidation stages [27,28]. In both cases, the system must operate at high temperatures to maximize thermal efficiency for power generation. However, a key challenges the sintering and degradation of OC materials. Additionally, significant temperature differences between the reduction and oxidation stages - which are inevitable given that the reduction stage is highly exothermic and the oxidation stage is endothermic - raise concerns about OC stability.

CLC operation can significantly differ when applied to the oxidation of pyrolysis gases, as the primary goal - efficient conversion of these gases into CO_2 and H_2O - does not require the high temperatures needed for power generation. Instead, a relatively low-temperature, stable heat source for pyrolysis would be sufficient. Under these conditions, some of the typical constraints limiting CLC systems, such as thermal stability and sintering of the OC, may not be as critical. To the best of our knowledge, the application of CLC systems for the oxidation of pyrolysis gases at relatively low temperatures (600–700 °C) has not been explored in the existing literature, as these temperature ranges are not typically relevant for power production. Indeed, only a few studies have investigated low-temperature CLC. Xu et al. used a CuO-based OC to fully oxidize the unconverted CO exiting a high-temperature CLC reactor [29]. Similarly, Güleç et al. performed CLC with Cu- and Mn-based oxides at around 500 °C to selectively remove organic contaminants from hot gas streams [30]. Based on these references, Cu- or Mn-based OCs appear to be the optimal choice for low-temperature CLC, as they demonstrate good conversion performance at lower temperatures and exhibit exothermic behavior - not only during their oxidation phase with air but also during the reduction phase with the main combustible pyrolysis gases (CH_4, CO, and H_2). This could enable stable operation without significant temperature fluctuations in the reaction system.

Given these considerations, the primary objective of this study is to evaluate the performance of a fixed-bed CLC reactor operating in the 600–650 °C temperature range, aimed at combusting a mixture of pyrolysis gases for CO_2 capture. The behavior of three different OC, in terms of combustion efficiency and performance over several redox cycles, has been assessed under varying weight hourly space velocities (WHSV) in the fixed bed. The objective of this study is to determine whether a CuO-based OC can fully oxidize pyrolysis gas over a specific period at lower temperatures than those typically used in the CLC processes, and in a fixed bed instead of the conventional CFB.

2. Experimental section

2.1. Materials

2.1.1. Oxygen carriers' preparation and characterization

The oxygen carriers (OC) used for the experiments were commercial grade CuO and carulite (mixed oxide of Mn_2O_3 and CuO [31]), both

from SigmaAldrich, and Al_2O_3 impregnated with CuO (nominal content of 20 wt%) prepared by incipient impregnation. For this preparation method, an aqueous solution containing 50 wt% ethanol was used. A specific amount of $Cu(NO_3)_2{\cdot}3H_2O$ was then added to the mixture, which was gradually applied to the Al_2O_3 spheres. The impregnated Al_2O_3 spheres were dried overnight at 105 °C and then calcined at 900 °C for 3 h. The averages particle sizes of the OCs were 0.50–1.25 mm for CuO, and 2–3 mm for both carulite and CuO/Al_2O_3.

The OC samples were characterized by inductively coupled plasma-optical emission spectrometry (ICP-OES) to determine the actual metal loadings, N_2 adsorption-desorption isotherms to determine the textural properties, X-ray diffraction (XRD) to evaluate the crystalline structure, H_2 temperature-programmed reduction (H_2-TPR) to study the reducible species, and field emission scanning electron microscopy (FESEM) combined with an energy-dispersive detector (EDS) to evaluate the surface morphology. The equipment employed and the conditions under which the analyses were conducted are detailed in the Supplementary Information.

2.1.2. Pyrolysis gas

To ensure controlled and reproducible conditions for the experiments, commercial gas mixture bottles were used. The gas compositions are detailed in Table 1. Gas 1 replicated the typical composition of pyrolysis gases observed in previous experiments conducted by the research group [15]. Gas 2, which features a simplified composition excluding C_2 hydrocarbons, was used in the CLC cyclic experiments.

Table 1
Composition of surrogate pyrolysis gas.

	Gas 1	Gas 2
Species	(% vol.)	(% vol.)
H_2	13.03	13.06
N_2	7.52	9.00
CH_4	12.98	12.99
CO	39.96	39.97
CO_2	25.00	24.98
C_2H_4	0.50	–
C_2H_6	0.51	–
C_2H_2	0.50	–

2.2. Experimental system and procedure

2.2.1. Fixed bed reactor setup

A schematic diagram of the fixed bed reactor system used is shown in Fig. 1. The experimental unit consisted of a gas feed zone, a reaction zone, and a product collection zone. The pyrolysis gas oxidation tests were conducted in a fixed-bed tubular stainless-steel reactor (inner diameter of 1.27 cm, length of 48 cm, and a distance of 26 cm from the sieve plate to the top of the reactor). The solid was placed on a sieve plate inside the reactor. The setup included three distinct gas inlets, each equipped with a mass flow controller. A valve system was used to select the gas to be introduced into the reactor (air, nitrogen, or surrogate pyrolysis gas). The reaction zone was heated by an electrical furnace, and the temperature was controlled by a K-type thermocouple, whose thermosensitive tip was positioned in contact with the OC bed exit. The products released during the pyrolysis gas oxidation process passed through a water-cooled condenser, where water condensed, and a cotton filter that removed small water droplets carried by the oxidized gas. Further downstream, a bubbler ensured flow presence and helped condense any remaining droplets. The volumetric composition (H_2, N_2, O_2, CO, CH_4, CO_2, C_2H_4, C_2H_6, and C_2H_2) of both the incoming and exiting gases was analysed online using an Agilent 3000-A micro-gas chromatograph.

2.2.2. Experimental procedure

The bed height was kept constant across all experiments (22 cm), resulting in a consistent occupied bed volume of 27.9 cm^3. Due to the differing densities of the OC materials used, the mass of each OC varied. Specifically, 23.5, 26.5 and 93.5 g of CuO, carulite and CuO/Al_2O_3 were employed, respectively.

The WHSV was calculated according to Eq. (1):

$$WHSV = \frac{\dot{m}_{gas}}{m_{OC,bed}} \quad \text{(Eq. 1)}$$

where $m_{OC,bed}$ is the mass of OC placed inside the reactor (g), and $\dot{m}_{gas}$ is the gas mass flow rate at the reactor inlet ($g{\cdot}h^{-1}$).

The experimental procedure varied depending on whether the operation was cyclic or not. In the non-cyclic experiments, the reactor bed was heated to the desired temperature in the 600–650 °C temperature range using the electric furnace, and air was introduced to ensure

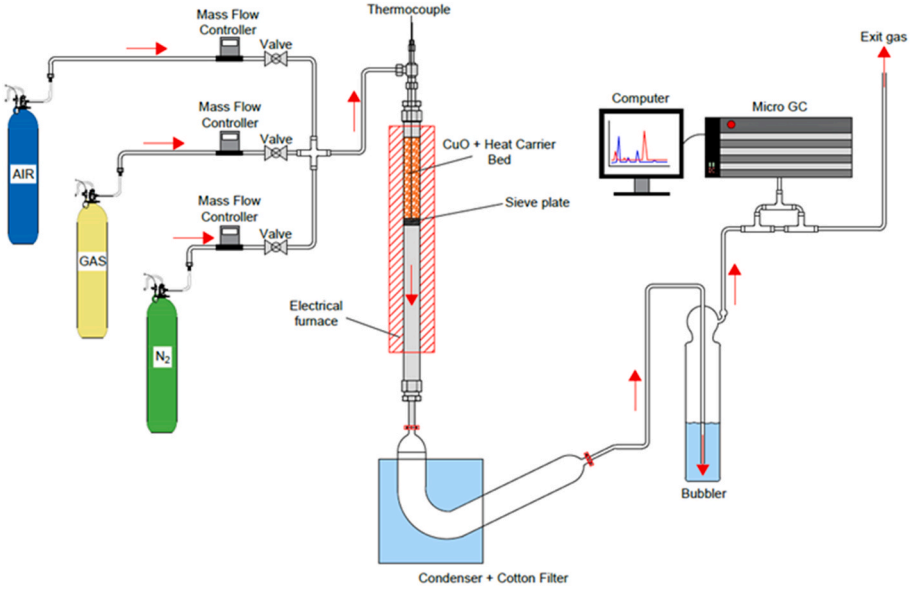

Fig. 1. Laboratory experimental setup scheme.

complete oxidation of the bed. Once the oxidation was complete, the air valve was closed, and pure N_2 was introduced to inert the reactor. After the reactor was inerted, the nitrogen valve was closed, and pyrolysis gas was introduced, marking the start of the experiment (the OC reduction and pyrolysis gas combustion phase in the CLC process). The experiments were conducted over a period of 45 min. The desired WHSV between 0.06 h^{-1} and 0.10 h^{-1} was achieved by adjusting the gas flow rate between 88 and 147 mL(STP)·min^{-1} for CuO, 25 and 42 mL(STP)·min^{-1} for carulite, and 22 and 37 mL(STP)·min^{-1} for CuO/Al_2O_3, respectively.

In the CLC cyclic experiments, the OC reduction (and consequently, the combustion of pyrolysis gas) and oxidation alternated. The procedure began with a fully oxidized and heated bed in an inerted reactor. Under these conditions, pyrolysis gas (Gas 2) was introduced for 20 min during the OC reduction step with a gas flow rate of 100 mL(STP)·min^{-1}, followed by a 13-min purge with pure N_2. An increase in WSHV (0.27 h^{-1}) was implemented to shorten the cycles, as it was observed that at lower flow rates, CuO/Al_2O_3 was able to completely oxidize the gases for over 30 min. Once the reactor was inerted again, the OC oxidation stage began, lasting 25 min (air flow rate of 300 mL(STP)·min^{-1}), followed by another 13-min purge with pure N_2. During the purges with pure N_2, which were performed each time the system switched from reduction to oxidation or vice versa, a flow rate of 200 mL(STP)·min^{-1} was introduced. This cycle was repeated with each subsequent CLC cycle following the same procedure.

Combustion efficiency and OC conversion were calculated for each experiment as main indicators of the system performance. The combustion efficiency of each experiment represents the ability of the system to convert fuel compounds (CO, CH_4, H_2 and C_2's, in the specific case of pyrolysis gases) to CO_2 and H_2O [32]. In all the experiments conducted, the total amount of gas passing through the CLC reactor was known, which allowed for the determination of the total moles of pyrolysis gas at each time point. Using these gas moles, the stoichiometric amount of oxygen required for complete combustion were calculated. Being the oxygen transport capacity of the OCs and the outlet gas compositions known, the evolution of the oxygen carrier conversion could be determined applying a calculation procedure analogous to that reported by Adánez-Rubio et al. in a batch fluidized bed [31]. This value was referred to as the OC conversion (reduction) percentage. Finally, for some of the experiments, a carbon balance of the gaseous species entering and leaving the reactor enabled the estimation of the amount of carbon deposition.

2.3. Experimental design

Table 2 provides a summary of the experiments conducted. A preliminary 'blank' experiment (corresponding to Block 0) was carried out at 625 °C using an unreactive glass wool bed to assess any potential changes in the surrogate gas composition caused by gas-phase reactions due to temperature and/or the catalytic effects of the reactor walls.

For each OC, the experiments corresponding to Block 1, Block 2 and Block 3 were planned according to a 2^2 full factorial design (FFD) to examine the influence of two independent factors - gas combustion temperature and WHSV - on a single dependent response variable: the OC combustion efficiency. This factorial design allowed for the simultaneous analysis of the main effects of the two independent factors, as well as their interaction (i.e., the effect of one factor depends on the level of the other). Each independent factor was evaluated at two distinct levels (four runs). The factors studied were gas combustion temperature, ranging from 600 to 650 °C, and WHSV, varying between 0.06 and 0.10 h^{-1}. To assess linearity and experimental variability, three additional replicates were conducted at the center point conditions (625 °C and 0.08 h^{-1}). In total, seven runs were performed for each OC. Each experiment lasted 45 min. The response variable was calculated as the area under the combustion efficiency percentage curve over the complete experiment (reduction phase of the CLC process). The experimental data were statistically analysed using analysis of variance (ANOVA) with a 95 % confidence level. It was assumed that the null hypothesis (i.e., the factor has an effect on the response variable) cannot be rejected when the p-value was less than or equal to 0.05.

To monitor the evolution of the bed over time, determine how long each OC could fully oxidize the pyrolysis gas, and investigate potential secondary reactions of the pyrolysis gas, three experiments were conducted. These 'long' experiments were performed at 625 °C and WSHV of 0.08 h^{-1} (Block 4). The duration of the experiments was not fixed; they ended when the gas output composition stabilized over a certain period, indicating that a steady state had been reached.

Finally, the Block 5 experiments (three runs) were designed to study the evolution of the OC bed for the best-performing OC across ten cycles at the three temperatures used in the previous experiments. Based on previous tests, the cycles were carried out in the following order: 1) reduction, 2) purge with N_2, 3) oxidation, and 4) purge with N_2. The total duration of each experiment was 12 h.

Table 2
Operating conditions of CLC tests.

	Experiment	OC	Temperature (°C)	WHSV (h^{-1})	Gas	Time (min)	Repetitions
0.1	Blank	–	625	0.08	Gas 1	45	1
1.1	CuO_600_006	CuO	600	0.06	Gas 1	45	1
1.2	CuO_650_006	CuO	650	0.06	Gas 1	45	1
1.3	CuO_600_010	CuO	600	0.10	Gas 1	45	1
1.4	CuO_650_010	CuO	650	0.10	Gas 1	45	1
1.5	CuO_625_008	CuO	625	0.08	Gas 1	45	3
2.1	Car_600_006	Carulite	600	0.06	Gas 1	45	1
2.2	Car_650_006	Carulite	650	0.06	Gas 1	45	1
2.3	Car_600_010	Carulite	600	0.10	Gas 1	45	1
2.4	Car_650_010	Carulite	650	0.10	Gas 1	45	1
2.5	Car_625_008	Carulite	625	0.08	Gas 1	45	3
3.1	Als_600_006	CuO/Al_2O_3	600	0.06	Gas 1	45	1
3.2	Als_650_006	CuO/Al_2O_3	650	0.06	Gas 1	45	1
3.3	Als_600_010	CuO/Al_2O_3	600	0.10	Gas 1	45	1
3.4	Als_650_010	CuO/Al_2O_3	650	0.10	Gas 1	45	1
3.5	Als_625_008	CuO/Al_2O_3	625	0.08	Gas 1	45	3
4.1	CuO_625_008_LongExp	CuO	625	0.08	Gas 1	Indeterminate	1
4.2	Car_625_008_LongExp	Carulite	625	0.08	Gas 1	Indeterminate	1
4.3	Als_625_008_LongExp	CuO/Al_2O_3	625	0.08	Gas 1	Indeterminate	1
5.1	Cycles_CLC_600_Gas 2	CuO/Al_2O_3	600	0.27	Gas 2	720	1
5.2	Cycles_CLC_625_Gas 2	CuO/Al_2O_3	625	0.27	Gas 2	720	1
5.3	Cycles_CLC_650_Gas 2	CuO/Al_2O_3	650	0.27	Gas 2	720	1

3. Results and discussion

3.1. Characterization of the oxygen carriers

The calculated theoretical oxygen transport capacities for the three OCs were 20.0 % for CuO, 6.7 % for carulite, and 5.8 % for CuO/Al_2O_3.

The XRD patterns of the fresh OCs (Figure S1) revealed the presence of various Cu-based structures. The CuO material showed both CuO and Cu_2O phases. The CuO/Al_2O_3 OCs displayed the presence of phases such as $CuAl_2O_4$, CuO, Al_2O_3, and corundum. In contrast, the phases in carulite were $CuMn_2O_4$, Mn_3O_4, MnO_2, and $Na_4Mn_9O_{18}$. The XRD patterns of the used OCs at 625 °C (Figure S2) illustrated the effects of the reductive atmosphere during the process. The CuO and carulite materials were fully reduced to Cu^0, and to Cu^0 and MnO, respectively. The CuO/Al_2O_3 material exhibited phases such as $CuAl_2O_4$, CuO, Al_2O_3, and corundum, indicating that it was not completely reduced during the process. The absence of Cu^0 signal may be attributed to the presence of highly dispersed Cu^0 on the material's surface. The XRD results for the CuO/Al_2O_3 material (Figure S3) did not show any significant differences.

The OCs were also analysed via N_2 adsorption (see Table S1 and Figures S4-S7). The specific surface area results of the fresh materials showed the following trendy: CuO/Al_2O_3 (54.4 m^2/g) > carulite (10.5 m^2/g) > CuO (4.9 m^2/g). For the OCs used at 625 °C, the highest specific surface area was observed in CuO/Al_2O_3 (39.3 m^2/g), followed by carulite (9.5 m^2/g) and CuO (8.6 m^2/g). The specific surface area trend of the CuO/Al_2O_3 material used at different temperatures was as follows: CuO/Al_2O_3-600 (47.6 m^2/g) > CuO/Al_2O_3-650 (40.8 m^2/g) ≈ CuO/Al_2O_3-625 (39.3 m^2/g). The types of isotherms for fresh OCs (Figure S4) were also studied [33]. The isotherm for CuO/Al_2O_3 (Type IV) was characteristic of mesoporous materials, while the isotherm for CuO (Type III) was typical of non-porous materials, and the isotherm for carulite (Type II) was indicative of nonporous or macroporous materials.

The H_2-TPR results (Figure S8, Table S2) revealed distinct reduction peaks for each OC. CuO showed peaks at 250 °C and 284 °C, CuO/Al_2O_3 at 181 °C, 212 °C, 387 °C, 534 °C, and 714 °C, and carulite at 282 °C, 313 °C, 534 °C, and 674 °C. The reduction events occurring at low temperatures were attributed to the reduction of Cu^{2+} to Cu^0 in highly dispersed particles. The higher reduction temperatures observed for the CuO/Al_2O_3 material could be attributed to the formation of spinel phases [34].

A more detailed characterization of the fresh and used OCs is provided in the Supplementary Information.

3.2. Blank experiment

The results of the blank experiment (glass wool bed) at 625 °C revealed significant changes in the outlet gas composition without the use of an OC bed, as shown in Table 3. The most notable difference was the decrease in CO and the increase in CO_2 concentration. This can be explained by the occurrence of the Boudouard reaction (r.1), whose equilibrium is around 700 °C [35]. Below this temperature, the reaction favors the formation of CO_2 and carbon, and is promoted by certain metal constituents in stainless steel, particularly nickel, under reducing environments [36]. Additionally, there was a decrease in the total C_2 concentrations, which could be explained by the cracking of the least stable species (C_2H_2 and C_2H_4), potentially leading to carbon deposition. The differences in H_2 and CH_4 were smaller and more challenging to correlate with other possible reactions.

$$2\,CO \rightleftharpoons C(s) + CO_2 \quad \Delta H = -175.52\ \frac{kJ}{mol} \qquad \text{(r. 1)}$$

A visual inspection revealed the presence of soot deposits on the reactor walls after the experiment. The extent of carbon deposition during the experiment under steady-state conditions was estimated to be 23.3 % of the incoming carbon into the reactor (determined by performing a C atomic balance on the inlet and outlet gases, as previously explained), which represents a considerable amount. Neither carbon deposition nor the changes in gas composition could be attributable to the CLC experiments. Therefore, subsequent analyses of the gas composition variation were conducted using the results from this blank experiment as a reference.

Table 3
Variation in gas composition compared to Gas 1 in the blank experiment.

	Inlet composition (Gas 1)[a]	Outlet composition[a]
Species	(% vol.)	(% vol.)
H_2	14.1	14.8 ± 0.3
CH_4	14.0	15.6 ± 0.3
CO	43.2	34.9 ± 0.5
CO_2	27.0	34.1 ± 0.4
C_xH_y	1.7	0.6 ± 0.1

[a] Gas composition provided on a N_2-free basis.

3.3. CuO performance

As earlier mentioned, a 2^2 experimental design was used to investigate the influence of gas combustion temperature, WHSV, and their interaction for each OC. The selected response variable was the CO_2 content in the outlet gas. For CuO, the coefficient of variation was 1.66 %, indicating good repeatability and low dispersion in the results. The results showed p-values of 0.15 for gas combustion temperature, 0.64 for WHSV, and 0.40 for the interaction between these variables. Therefore, based on the chosen confidence level, it could not be concluded that either of the two factors or their interaction had a statistically significant effect on the response variable combustion efficiency.

Fig. 2a shows the temporal evolution of combustion efficiency for CuO (Block 1 experiments). Complete oxidation of the pyrolysis gas was not achieved at any point with this OC. Although CuO did not reach full oxidation, higher temperatures resulted in a more efficient CLC process [37], leading to greater combustion efficiency of the pyrolysis gases. While this may seem intuitive, CLC processes are typically conducted at much higher temperatures than those evaluated in the present study, as previously discussed, making the behavior observed at these lower temperatures particularly interesting. In particular, improved oxidation was observed with increasing temperature at WHSV of 0.06 h^{-1}. At WHSV of 0.08 h^{-1}, oxidation was slightly better at 650 °C than at 600 °C only during the first 15 min. Additionally, a significant increase in combustion efficiency was observed when the temperature was raised from 600 °C to 625 °C, but the increase was less pronounced when further raised to 650 °C. This is evident in Fig. 2a, where efficiency values for 0.08 h^{-1} at 625 °C were closer to those at 650 °C than at 600 °C. This suggested that a 25 °C increase, even with higher flow (higher WHSV), resulted in combustion efficiency values more similar to those observed with lower flow at higher temperature. The combustion efficiency increased with higher WHSV, regardless of the gas combustion temperature. CuO showed no sharp decline in combustion efficiency, a phenomenon attributed to the availability of oxygen in this bed through the whole experiment time. This suggested that the residence times used were adequate within the experimental limits for the WHSV applied.

Fig. 2b depicts the evolution of the oxygen carrier conversion for CuO. In general, the OC conversion increased almost linearly over time when sufficient oxygen was available from the OC. The bed conversion (OC reduction) during the experiment was minimal in all cases, reaching less than 20 % of the theoretical value under the experimental conditions studied.

To determine the point at which the OC conversion became limiting, long-duration experiments - where steady state was approached and all oxygen in the OC bed was assumed to have been consumed – were used (Block 4 experiments). Fig. 2c shows this long-term evolution of the gas

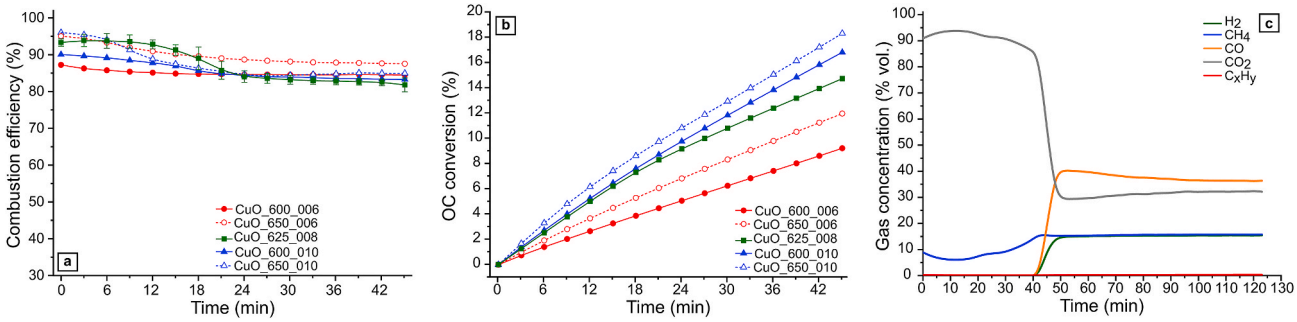

Fig. 2. Performance of CuO. a) Transient evolution of the combustion efficiency under different gas combustion temperature and WHSV conditions. b) Percentage of OC consumed during the experiments. c) Transient evolution of the volumetric concentration of the gas species (N_2 free basis) at the CLC reactor outlet (Block 4: 625 °C, 0.08 h^{-1}).

composition exiting from the CuO bed (625 °C and 0.08 h^{-1}). Interestingly and unlike for shorter experiments, a sudden drop in CO_2 concentration occurred around the 45-min mark. This drop would imply a corresponding drop in combustion efficiency, marking the interval when the bed has exhausted all available oxygen for reactions. This time will be referred to hereafter as t_B (breakthrough time corresponding to 'bed exhaustion'). The least reactive species in the pyrolysis gas was CH_4, which persisted from the beginning, with CuO unable to fully oxidize it. Other species only appeared when the combustion efficiency dropped sharply, indicating that oxidation had ceased. The already mentioned sharp decline in combustion efficiency at t_B=45 min corresponds to an OC conversion of approximately 14 % in Fig. 2b. Thus, it can be concluded that this conversion was close to the maximum achievable OC conversion at 625 °C and 0.08 h^{-1}. This suggests that CuO provided very limited oxygen availability relative to the theoretical value, likely due to mass transfer limitations. The low specific surface area of this material supported this observation.

3.4. Carulite performance

For carulite, the results showed p-value <0.01 for gas combustion temperature, 0.01 for WHSV, and 0.03 for their interaction, indicating that both factors had a statistically significant effect on the combustion efficiency, and that the effect of each was dependent on the level of the other. The percentage of area increased as the gas combustion temperature rose. In contrast, this variable decreased with increasing WHSV at 600 °C, while no effect of WHSV was observed at 650 °C.

High temperatures and low WHSV values produced the best results in terms of combustion efficiency, as can be seen in Fig. 3a. Nearly complete combustion of the pyrolysis gases was achieved at 650 °C and 0.06 h^{-1} throughout the experiment. Under all the experimental conditions, combustion efficiencies decreased over time. A decrease in temperature exerted a more significant negative effect on combustion efficiency than an increase in WHSV. Fig. 3c shows that the oxygen carrier conversion linearly increased over the duration of the experiment, but as already seen for CuO, it was still far from reaching high values.

Carulite demonstrated better overall performance than CuO in oxidizing gases over an extended period (Block 4 experiments), as shown in Fig. 3c. The sharp drop in CO_2 concentration (t_B) occurred at 210 min. However, and accordingly to combustion efficiency under those conditions, CO_2 concentration steadily declined from the beginning of the experiment. Regarding the combustible gases, CH_4, once again, appeared first and was the least reactive species, whereas CO and H_2 did not appear until after the aforementioned CO_2 sharp decrease.

A theoretical linear extrapolation of the observed OC conversion for 625 °C and 0.08 h^{-1} (Fig. 3b) to t_B would suggest a bed conversion of around 54 % of the theoretical maximum at this time. Although not as low as that of CuO, the limited OC conversion could also be attributed to the unavailability of a significant fraction of oxide constituents due to mass transfer limitations and low specific surface area. It is important to note that in the case of this material, bed conversion would involve the reduction of both theoretically active metal oxides (Cu and Mn) that are part of its composition.

3.5. CuO/Al_2O_3 performance

The results obtained with CuO/Al_2O_3 as the OC indicated that only the WHSV significantly influenced the CO_2 content at the outlet (p-value <0.01). The p-values for gas combustion temperature and the interaction between temperature and WHSV (both 0.09) suggested that, at a 95 % confidence level, no significant statistical effect could be inferred from the variation of both parameters. Graphically, this result can be clearly seen in Fig. 4a, where the behavior of combustion efficiencies in experiments conducted at equal temperatures (600 and 650 °C) was very similar, with combustion efficiencies decreasing earlier at higher WHSV values. Combustion efficiencies remained at 100 % for all experimental

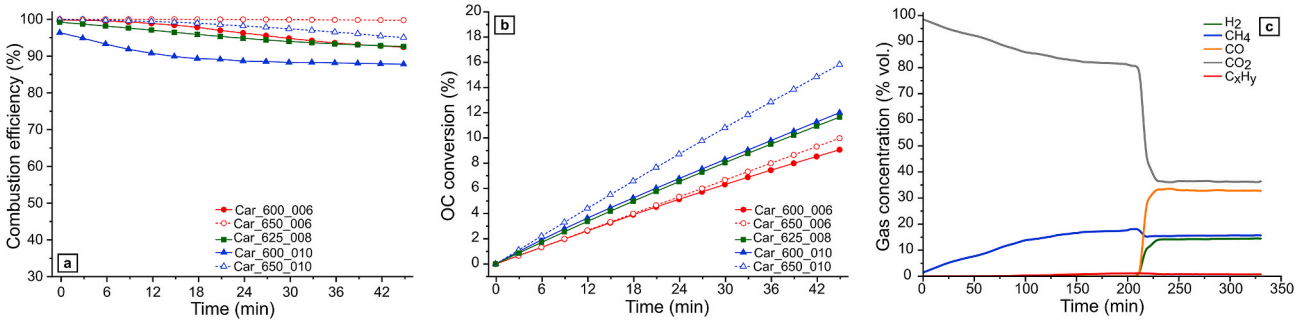

Fig. 3. Performance of carulite. a) Transient evolution of the combustion efficiency under different gas combustion temperature and WHSV conditions. b) Percentage of OC consumed during the experiments. c) Transient evolution of the volumetric concentration of the gas species (N_2 free basis) at the CLC reactor outlet (Block 4: 625 °C, 0.08 h^{-1}).

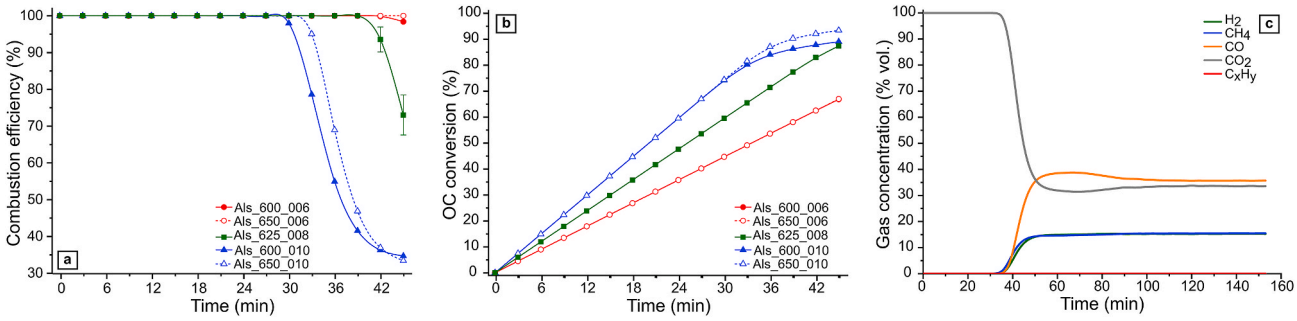

Fig. 4. Performance of CuO/Al_2O_3. a) Transient evolution of the combustion efficiency under different gas combustion temperature and WHSV conditions. b) Percentage of OC consumed during the experiments. c) Transient evolution of the volumetric concentration of the gas species (N_2 free basis) at the CLC reactor outlet (Block 4: 625 °C, 0.08 h^{-1}).

conditions for most of the experiment duration. For comparison, a similar behavior was only observed for carulite at 650 °C and 0.06 h^{-1}. At WHSV of 0.10 h^{-1}, combustion efficiency rapidly declined at around 30 min, whereas at 0.06 h^{-1}, this decay began more gradually towards the end of the experiments (45 min).

OC conversions (Fig. 4b) were consistent with the evolution of combustion efficiencies. Conversions linearly increased, reaching values over 80 % of the theoretical value in the most favorable cases (T ≥ 625 °C), and gradually declined afterwards. Achieving such high conversions indicated the availability of a major fraction of the metal oxide in the OC, unlike CuO and carulite, and demonstrated a higher dispersion of the active CuO phase onto the Al_2O_3 support, as suggested by the specific surface area values (see Table S1). In Fig. 4b, a more noticeable gradual decline in OC conversion for space velocities of 0.06 h^{-1} began around 80 %, coinciding with the onset of the combustion efficiency decay shown in Fig. 4a.

Fig. 4c shows that at the intermediate WHSV of 0.08 h^{-1} and 625 °C, the distinctive feature of CuO/Al_2O_3 was the complete conversion of all pyrolysis gases, including CH_4, from the beginning. Since CH_4 was the most recalcitrant gas towards oxidation under the conditions of this study, this confirmed the superior performance of CuO/Al_2O_3 in oxidizing pyrolysis gases. A sharp drop in CO_2 concentration occurred at t_B of around 40 min. This corresponds to an incipient decline in the OC conversion at around 80 % for these experimental conditions (Fig. 4b).

3.6. CLC cycles

As demonstrated, the OC with the best performance was CuO/Al_2O_3. Therefore, this OC was selected for a series of experiments to observe its behavior in CLC cycles (Block 5). Fig. 5 presents the results of the CLC cycles conducted at 650 °C. Each experiment lasted approximately 12 h, during which ten complete cycles were performed. In all cycles, the gas was almost fully oxidized (with only CO_2 evolving out of the bed, reaching 90 %, and the remaining 10 % primarily N_2). Notably, no performance degradation was observed throughout the cycles. However, some carbon deposition was detected, indicated by the appearance of small CO_2 peaks during each air oxidation stage. A preliminary estimate of the extent of carbon deposition under these conditions is presented in the following section.

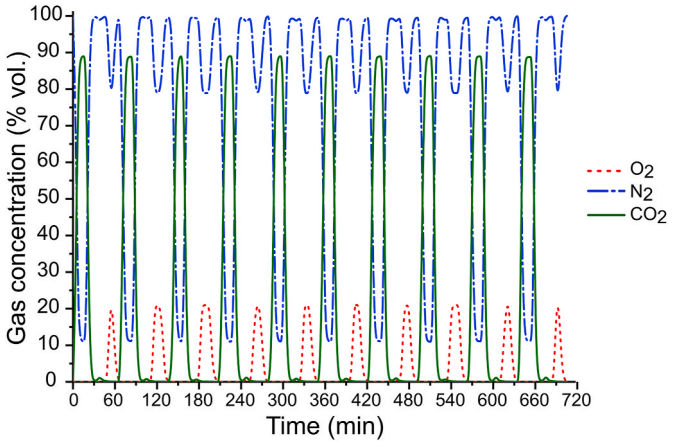

Fig. 5. Gas composition during the CLC cycles with CuO/Al_2O_3 at 650 °C. (For interpretation of the references to colour in this figure legend, the reader is referred to the Web version of this article.)

3.7. Carbon deposition

Carbon deposition was detected on all the three OCs used, as evidenced by the FESEM images. Fig. 6 shows micrographs of the used CuO/Al_2O_3. An overview of the surface of this spent OC is presented in Fig. 6a and 6b (more detailed view of the material's surface using the angle selective backscattered -AsB- signal). First, both figures revealed a high metallic dispersion on the surface of the Al_2O_3 support, which may contribute to the superior performance of this material, as noted in the previously presented results. Second, details in Fig. 6c and 6d (in-lens and Asb modes, respectively) revealed the occurrence of carbon deposition. The elongated structures shown in Fig. 6c, a shape commonly associated with the formation of carbon nanotubes, could also be attributed to carbon deposition. For CuO, carbon deposition was significantly higher, as depicted in Figure S12 and visible at plain sight (Fig. 7). In contrast, it was less evident for carulite (Figure S13).

For the best-performing material, CuO/Al_2O_3, and under the experimental conditions corresponding to Fig. 5 (reduction-oxidation cycles), a preliminary quantification of the extent of carbon deposition was estimated. Based on the chromatographic analysis, the amount of deposited carbon (as a percentage of the total carbon fed to the system during the gas combustion step) was calculated. Approximately 1 % of the total carbon fed into the system was deposited onto the OC (see Table 4). No significant differences were found between cycles, suggesting that the amount of carbon deposition did not increase with continued OC use. Furthermore, no significant variation was found across the studied temperature range of 600–650 °C. Carbon deposition has been reported in copper-based OCs using methane as a fuel in CLC systems, although to a lesser extent that with other metal oxides, such as those based on Ni and Fe, for instance Ref. [38]. Additionally, carbon deposition can be fully suppressed if water vapor is fed into the system [39]. Although synthetic gas without H_2O was used in this study, real pyrolysis gas would contain some water vapor after condensation of organic vapors, which could partially or even totally inhibit carbon deposition.

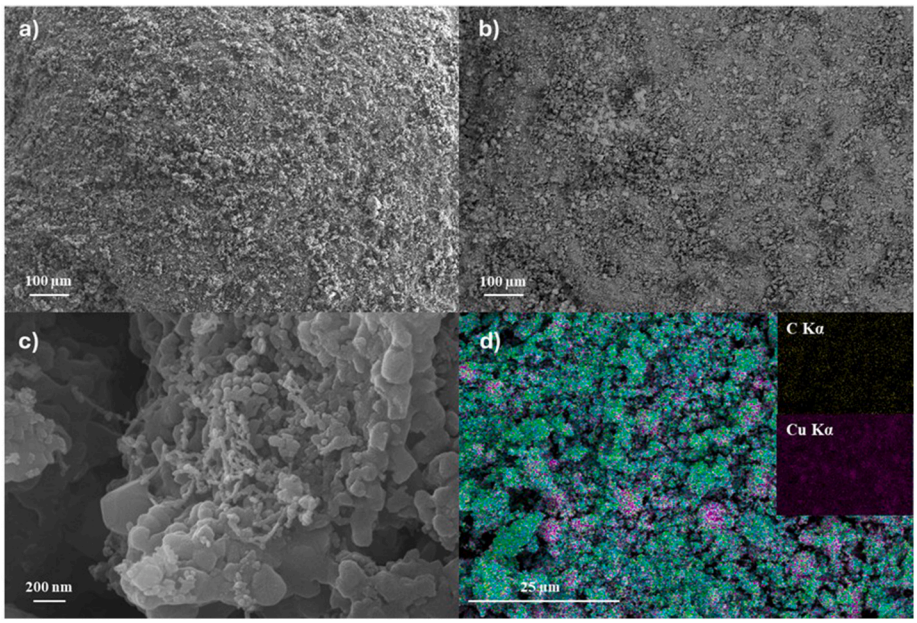

Fig. 6. FESEM images of CuO/Al_2O_3 used OC a) and c) obtained from in-lens signal, b) AsB signal, and d) mapping of the surface of used CuO/Al_2O_3.

Fig. 7. Carbon deposition after an experiment with a CuO bed (experiment 4.1).

Table 4
Extent of carbon deposition onto the CuO/Al_2O_3 carrier in the cyclic experiments.

Temperature (°C)	Average C deposition per cycle[a] (%)
600	1.0 ± 0.4
625	1.2 ± 0.4
650	0.8 ± 0.2

[a] As % of total C fed into the reactor.

4. Conclusions

In this study, the impact of gas combustion temperature and weight hourly space velocity (WHSV) on the chemical looping combustion (CLC) of pyrolysis gas was investigated using three oxygen carriers (OCs): CuO, carulite, and CuO/Al_2O_3. The experimental results revealed significant differences in the performance of each OC.

For CuO, neither the gas combustion temperature nor WHSV significantly affected the combustion efficiency. In contrast, both gas combustion temperature and WHSV, along with their interaction, were found to significantly influence the combustion efficiency for carulite. Notably, increasing the gas combustion temperature improved the conversion efficiency, while higher WHSV tended to reduce the combustion efficiency at lower temperature, with minimal impact at higher temperatures. For CuO/Al_2O_3, only WHSV significantly affected CO_2 content.

The transient behavior of combustion efficiency indicated that CuO/Al_2O_3 was the most effective OC, fully oxidizing the pyrolysis gas. In contrast, CuO exhibited the lowest combustion rates, while carulite performed similarly to CuO/Al_2O_3 at high temperatures, although oxygen depletion occurred more rapidly. The total OC conversion confirmed that CuO/Al_2O_3 achieved the highest oxygen consumption. A noticeable drop in CO_2 was observed when the oxygen content in the bed reached approximately 90 %. Conversely, neither CuO nor carulite showed such decline during the 45-min experiments.

The CLC cycles performed with CuO/Al_2O_3 at 650 °C exhibited stable performance over multiple cycles, maintaining consistent oxidation efficiency without any performance degradation throughout the 12-h experiment (10 reduction-oxidation cycles).

Further analysis of the OC beds revealed that carbon deposition occurred for the three tested OCs, particularly in the case of CuO, as evidenced by FESEM images and evolution of CO_2 during OCs oxidation with air. For CuO/Al_2O_3, approximately 1 % of the total carbon fed per cycle was deposited as carbon. However, this phenomenon did not appear to significantly influence the OC performance over successive cycles.

These findings suggest that CuO/Al_2O_3 was the most promising OC for efficient oxidation in CLC applications, demonstrating stable long-term performance. The study also underscored the importance of optimizing operational conditions, such as gas combustion temperature and WHSV, to enhance the performance of different OCs.

CRediT authorship contribution statement

César Gracia-Monforte: Writing – original draft, Methodology, Investigation, Data curation, Conceptualization. **Francisco Maldonado-Martín:** Writing – review & editing, Methodology. **María Atienza-Martínez:** Writing – review & editing, Investigation, Data curation. **Javier Ábrego:** Writing – original draft, Project administration, Investigation, Data curation, Conceptualization.

Acknowledgements

This work was funded by the Spanish Agencia Estatal de Investigación (AEI) and Ministerio de Ciencia e Innovación (MICINN), and the European Union's NextGenerationEU funds and Plan de Recuperación, Transformación y Resiliencia (grant number PDC2022-133374-I00). María Atienza-Martínez would like to thank Dirección General de Industria, Energía y Proyectos Estratégicos S4, Gobierno de Navarra, and European Regional Development Fund (ERDF) for supporting her postdoctoral contract (grant number 0011-1365-2023-000101). Open access funding provided by Universidad Pública de Navarra.

Appendix A. Supplementary data

Supplementary data to this article can be found online at https://doi.org/10.1016/j.biombioe.2025.107911.

Data availability

Data will be made available on request.

References

[1] J.A. Garcia-Nunez, M.R. Pelaez-Samaniego, M.E. Garcia-Perez, I. Fonts, J. Abrego, R.J.M. Westerhof, M. Garcia-Perez, Historical developments of pyrolysis reactors: a review, Energy Fuels 31 (6) (2017) 5751–5775, https://doi.org/10.1021/acs.energyfuels.7b00641.

[2] Y. Li, S.K. Khanal, Bioenergy: Principles and Applications, first ed., Wiley-Blackwell, New Jersey, 2016.

[3] A.V. Bridgwater, Biomass fast pyrolysis, Bioresour. Technol. 8 (2) (2004) 21–50, https://doi.org/10.2298/TSCI0402021B.

[4] A. Pivato, H. Gohar, D.L. Antille, A. Schievano, G. Beggio, P. Reichardt, F. Di Maria, W. Peng, S. Castegnaro, M.C. Lavagnolo, Air-polluting emissions from pyrolysis plants: a systematic mapping, Environments 11 (7) (2024) 1–24, https://doi.org/10.3390/environments11070149.

[5] K. Crombie, O. Mašek, Investigating the potential for a self-sustaining slow pyrolysis system under varying operating conditions, Bioresour. Technol. 162 (2014) 148–156, https://doi.org/10.1016/j.biortech.2014.03.134.

[6] Intergovernmental Panel on Climate Change (IPCC), Climate Change 2022: Mitigation of Climate Change, 2023.

[7] T. Mendiara, A. Navajas, A. Abad, T. Pröll, M. Munárriz M., L.M. Gandía, F. García-Labiano, L.F. de Diego, Life cycle assessment of wheat straw pyrolysis with volatile fractions chemical looping combustion, Sustainability 16 (10) (2024) 4013, https://doi.org/10.3390/su16104013.

[8] M.J. Antal, M. Grønli, The art, science, and technology of charcoal production, Ind. Eng. Chem. Res. 42 (8) (2003) 1619–1640, https://doi.org/10.1021/ie0207919.

[9] H.P. Schmid, C. Kammann, N. Hagemann, J. Leifeld, T.D. Bucheli, M.A. Sánchez Monedero, M.L. Cayuela, Biochar in agriculture – a systematic review of 26 global meta-analyses, GCB Bioenergy 13 (11) (2021) 1708–1730, https://doi.org/10.1111/gcbb.12889.

[10] International Biochar Initiative, Global biochar market report. https://145249425.hs-sites-eu1.com/2023-global-biochar-market-report, 2023. (Accessed 19 December 2023).

[11] Charm industrial. https://charmindustrial.com/2023. (Accessed 19 December 2023).

[12] Charm Industrial, Inside Charm Industrial's big bet on corn stalks for carbon removal. https://www.technologyreview.com/2022/05/26/1052671/charm-industrials-carbon-removal-corn/, 2022. (Accessed 10 October 2022).

[13] H.P. Schmidt, A. Anca-Couce, N. Hagemann, C. Werner, D. Gerten, W. Lucht, C. Kammann, Pyrogenic carbon capture and storage, GCB Bioenergy 11 (4) (2019) 573–591, https://doi.org/10.1111/gcbb.12553.

[14] E. Hoekstra, R.J.M. Westerhof, W. Brilman, W.P.M. Van Swaaij, S.R.A. Kersten, K.J. A. Hogendoorn, M. Windt, Heterogeneous and homogeneous reactions of pyrolysis vapors from pine wood, AIChE J. 58 (9) (2012) 2830–2842, https://doi.org/10.1002/aic.12799.

[15] J. Ábrego, M. Atienza-Martínez, F. Plou, J. Arauzo, Heat requirement for fixed bed pyrolysis of beechwood chips, Energy 178 (2019) 145–157, https://doi.org/10.1016/j.energy.2019.04.078.

[16] C. Di Blasi, C. Branca, F. Masotta, E. De Biase, Experimental analysis of reaction heat effects during beech wood pyrolysis, Energy Fuels 27 (5) (2013) 2665–2674, https://doi.org/10.1021/ef4001709.

[17] J. Adánez, A. Abad, F. Garcia-Labiano, P. Gayan, L.F. de Diego, Progress in chemical-looping combustion and reforming technologies, Prog. Energy Combust. Sci. 38 (2) (2012) 215–282, https://doi.org/10.1016/j.pecs.2011.09.001.

[18] H. Jiang, R. Huo, Z. Zhang, Y. Lin, Z. Zhao, Z. Huang, Y. Fang, H. Li, Removal of pollution from the chemical looping process: a mini review, Fuel Process. Technol. 221 (2021) 106937, https://doi.org/10.1016/j.fuproc.2021.106937.

[19] R.J. Thorne, E.A. Bouman, K. Sundseth, A. Aranda, T. Czakiert, J.M. Pacyna, E. G. Pacyna, M. Krauz, A. Celińska, Environmental impacts of a chemical looping combustion power plant, Int. J. Greenh. Gas Control 86 (2019) 101–111, https://doi.org/10.1016/j.ijggc.2019.04.011.

[20] D. Hu, G. Cao, M. Du, J. Huang, J. Zhao, C. Li, Y. Fang, Insight into the biomass pyrolysis volatiles reaction with an iron-based oxygen carrier in a two-stage fixed-bed reactor, Chem. Eng. J. 465 (2023) 142860, https://doi.org/10.1016/j.cej.2023.142860.

[21] D. Hu, J. Huang, J. Zhao, Z. Wang, Z. Yu, H. Xiao, H. Bai, C. Li, Y. Fang, Reaction characteristics of Shenmu coal pyrolysis volatiles with an iron-based oxygen carrier in a two-stage fixed-bed reactor, Fuel Process. Technol. 235 (2022) 107371, https://doi.org/10.1016/j.fuproc.2022.107371.

[22] L. Chen, H. Li, H. Wang, K. Liu, Performance of red mud oxygen carriers in chemical-looping hydrogen production using different components of plastic waste pyrolytic gas, J. Clean. Prod. 409 (2023) 137213, https://doi.org/10.1016/j.jclepro.2023.137213.

[23] Y. Sun, B. Dong, L. Wang, H. Li, E. Thorin, Technology selection for capturing CO_2 from wood pyrolysis, Energy Convers. Manag. 266 (2022) 115835, https://doi.org/10.1016/j.enconman.2022.115835.

[24] J.P. Polin, C.A. Peterson, L.E. Whitmer, R.G. Smith, R.C. Brown, Process intensification of biomass fast pyrolysis through autothermal operation of a fluidized bed reactor, Appl. Energy 249 (2019) 276–285, https://doi.org/10.1016/j.apenergy.2019.04.154.

[25] S. Daneshmand-Jahromi, M.H. Sedghkerdar, N. Mahinpey, A review of chemical looping combustion technology: fundamentals, and development of natural, industrial waste, and synthetic oxygen carriers, Fuel 341 (2023) 12762, https://doi.org/10.1016/j.fuel.2023.127626.

[26] R. Naqvi, O. Bolland, Multi-stage chemical looping combustion (CLC) for combined cycles with CO_2 capture, Int. J. Greenh. Gas Control 1 (1) (2007) 19–30, https://doi.org/10.1016/S1750-5836(07)00012-6.

[27] S. Noorman, M. Van Sint Annaland, H. Kuipers, Packed bed reactor technology for chemical-looping combustion, Ind. Eng. Chem. Res. 46 (12) (2007) 4212–4220, https://doi.org/10.1021/ie061178i.

[28] K. Toffolo, S. Meunier, L. Ricardez-Sandoval, Optimal operation of a large-scale packed bed chemical-looping combustion process using nonlinear model predictive control, Fuel 357 (2024) 129876, https://doi.org/10.1016/j.fuel.2023.129876.

[29] L. Xu, Z. Li, H. Sun, J. Bao, N. Cai, Low-temperature chemical looping combustion for removing unburnt gaseous components with a cement-supported CuO oxygen carrier, Energy Fuels 27 (11) (2013) 6872–6879, https://doi.org/10.1021/ef401035b.

[30] F. Güleç, W. Meredith, C.-G. Sun, C.E. Snape, Selective low temperature chemical looping combustion of higher alkanes with Cu- and Mn- oxides, Energy 173 (2019) 658–666, https://doi.org/10.1016/j.energy.2019.02.099.

[31] I. Adánez-Rubio, A. Abad, P. Gayán, I. Adánez, L.F. de Diego, F. García-Labiano, J. Adánez, Use of hopcalite-derived Cu–Mn mixed oxide as oxygen carrier for chemical looping with oxygen uncoupling process, Energy Fuel. 30 (7) (2016) 5953–5963, https://doi.org/10.1021/acs.energyfuels.6b00552.

[32] A. Coppola, F. Scala, Chemical looping for combustion of solid biomass: a review, Energy Fuels 35 (23) (2021) 19248–19265, https://doi.org/10.1021/acs.energyfuels.1c02600.

[33] M. Thommes, K. Kaneko, A.V. Neimark, J.P. Olivier, F. Rodriguez-Reinoso, J. Rouquerol, K.S.W. Sing, Physisorption of gases, with special reference to the evaluation of surface area and pore size distribution (IUPAC Technical Report), Pure Appl. Chem. 87 (9–10) (2015) 1051–1069, https://doi.org/10.1515/pac-2014-1117.

[34] F.F. Barbosa, S.B.C. Pergher, T.P. Braga, Synergistic effects on Cu, Zn and Al-based catalyst: tracking the change of active sites during glycerol dehydration, Braz. J. Chem. Eng. (2024), https://doi.org/10.1007/s43153-024-00480-w.

[35] M. Tangstad, J.P. Beukes, J. Steenkamp, E. Ringdalen, 14 - coal-based reducing agents in ferroalloys and silicon production, in: I. Suárez-Ruiz, M.A. Diez, F. Rubiera (Eds.), New Trends in Coal Conversion. Combustion, Gasification, Emissions, and Coking, Woodhead Publishing, 2019, pp. 405–438.

[36] Y. Kwon, J.E. Eichler, M.E. Floto, L.A. Smith, A.M. Satkoski, C.B. Mullins, A study of refractory carbon deposits on Ni/Al_2O_3 catalysts for dry reforming of methane, ChemistrySelect 8 (2023) e202203734, https://doi.org/10.1002/slct.202203734.

[37] C.R. Forero, P. Gayán, F. García-Labiano, L.F. de Diego, A. Abad, J. Adánez, High temperature behaviour of a $CuO/\gamma Al_2O_3$ oxygen carrier for chemical-looping combustion, Int. J. Greenh. Gas Control 5 (4) (2011) 659–667, https://doi.org/10.1016/j.ijggc.2011.03.005.

[38] X. Cheng, Z. Gu, F. Li, X. Zhu, Y. Wei, M. Zheng, D. Tian, H. Wang, K. Li, Enhanced resistance to carbon deposition in chemical-looping combustion of methane: synergistic effect of different oxygen carriers via sequence filling, Chem. Eng. J. 421 (1) (2021) 129776, https://doi.org/10.1016/j.cej.2021.129776, 2021.

[39] X. Huang, X. Wang, M. Fan, Y. Wang, H. Adidharma, K.A.M. Gasem, M. Radosz, A cost-effective approach to reducing carbon deposition and resulting deactivation of oxygen carriers for improvement of energy efficiency and CO_2 capture during methane chemical-looping combustion, Appl. Energy 193 (2017) 381–392, https://doi.org/10.1016/j.apenergy.2017.02.059.